Chip

Research Article

PHOTONICS

DOI: 10.1016/j.chip.2021.100001

Generation and dynamic manipulation of frequency degenerate polarization entangled Bell states by a silicon quantum photonic circuit

Dong-Ning Liu[1,†], Jing-Yuan Zheng[1,†], Ling-Jie Yu[1,†], Xue Feng[1], Fang Liu[1], Kai-Yu Cui[1], Yi-Dong Huang[1,2] & Wei Zhang[1,2,*]

[1]*Frontier Science Center for Quantum Information, Beijing Innovation Center for Future Chips, Beijing National Research Center for Information Science and Technology (BNRist), Electronic Engineering Department, Tsinghua University, Beijing 100084, China* [2]*Beijing Academy of Quantum Information Sciences, Beijing 100193, China*

E-mail: zwei@tsinghua.edu.cn (Wei Zhang)

Cite as: Liu, D.-N. *et al. Chip* **1**, 1 (2022).
https://doi.org/10.1016/j.chip.2021.100001

[†]These authors have equal contributions on this work.

Received: 3 November 2021

Accepted: 1 December 2021

Published online: 16 February 2022

A silicon quantum photonic circuit was proposed and realized for the generation and the dynamic manipulation of telecom-band frequency-degenerate polarization entangled Bell states. Frequency degenerate biphoton states were generated in four silicon waveguides by spontaneous four wave mixing. They were transformed to polarization entangled Bell states through on-chip quantum interference and quantum superposition, and then coupled to optical fibers. The property of polarization entanglement in generated photon pairs was demonstrated by two-photon interference under two non-orthogonal polarization bases. The output state could be dynamically switched between two Bell states, which was demonstrated by the simplified Bell state measurement. The experiment results indicated that the manipulation speed supported a modulation rate of several tens kHz, showing its potential on applications of quantum communication and quantum information processing requiring Bell state encoding and dynamic control.

Keywords: Quantum information processing, Silicon quantum photonic circuits, Spontaneous four wave mixing, Quantum interference, Bell states

INTRODUCTION

Silicon photonics based on silicon-on-insulator (SOI) platform is a promising route for quantum photonic circuit, which can realize complicated on-chip photonic quantum information systems with large scalability and high stability[1–5]. On one hand, silicon waveguides are good $\chi^{(3)}$ nonlinear media at telecom band. By spontaneous four wave mixing (SFWM), high-quality correlated biphoton state could be generated in silicon waveguides of several millimeters[6–8]. The generation efficiency can be further improved if resonances in devices composed of silicon waveguides are used, such as micro-ring resonators[9–12]. On the other hand, silicon photonics based on SOI platform is compatible with the complementary metal oxide semiconductor (CMOS) technology[13,14]. Silicon photonic circuits based on on-chip interferometers have been developed for quantum state manipulation through quantum interference[15–17]. The quantum interference in these interferometers is controlled by phase shifters. Combining SFWM in silicon waveguides and silicon photonic circuit for quantum state manipulation, telecom-band quantum light sources for various biphoton state generation have been realized[18,19]. These works showed that the output states of silicon quantum photonic circuits can be controlled by on-chip phase shifters. However, the dynamic process of on-chip quantum state manipulation has not been demonstrated.

To show the potential of dynamic quantum state manipulation on silicon quantum photonic circuits, we focus on the quantum light source for frequency degenerate polarization entangled Bell state generation and manipulation in this work. It is well known that information can be encoded by these Bell states and decoded by Bell state measurement (BSM) based on linear optics[20], which have been widely used in experiments of quantum dense coding[21] and entanglement-based quantum secure direct communication[22]. Traditionally, polarization entangled biphoton states are generated by spontaneous parametric down conversion (SPDC) in nonlinear crystals[23,24]. Recently, biphoton state generation by SPDC in $\chi^{(2)}$ waveguides, such as periodically poled nonlinear crystal waveguides[25], GaAs waveguides[26] and SFWM in SiN waveguides[27] have developed rapidly, showing their potentials on different material platforms for integrated quantum photonics. To realize quantum light sources for polarization entangled biphoton states by silicon quantum photonic circuits, several schemes based on SFWM in silicon waveguides have been proposed and demonstrated[7,28,29]. In silicon waveguides, the fundamental quasi-transverse electrical (quasi-TE) mode is preferred in the biphoton state generation, since the efficiency of SFWM in this mode is much higher than that in other modes[30]. Hence, specific designs are required to realize the quantum superposition of biphoton states with orthogonal polarization directions, such as a modified Sagnac loop[7], a polarization rotator embedded in the middle of the silicon waveguide[28], or two-dimensional gratings[29]. However, in these schemes, only one mono-color pump light

DOI: 10.1016/j.chip.2021.100001

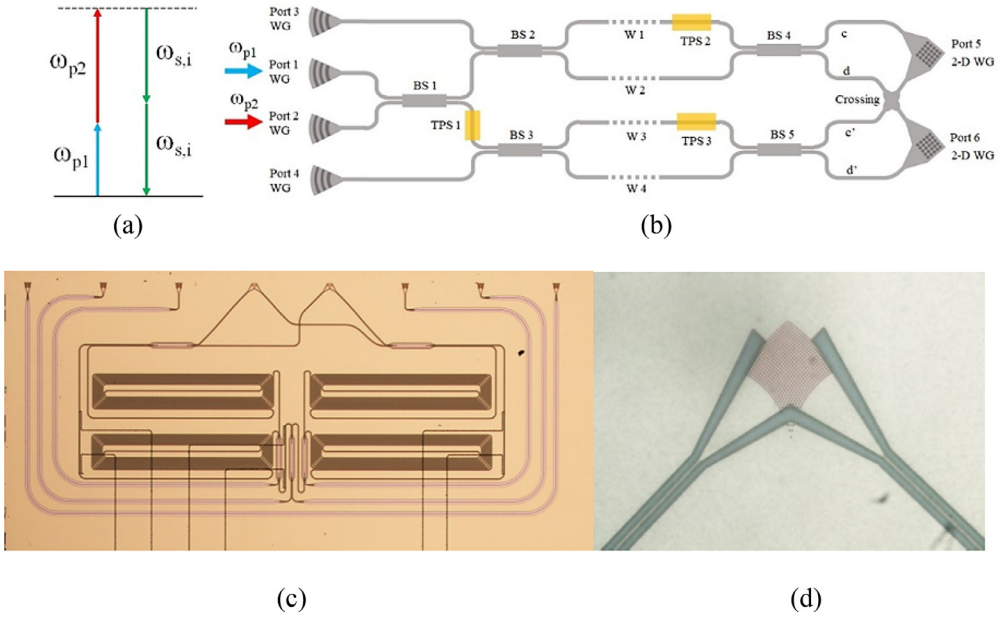

Fig. 1 | The silicon quantum photonic circuit for polarization entangled Bell state generation and dynamic manipulation. (a) SFWM under the non-degenerate pumping scheme. **(b)** Circuit design of the quantum light source. WG: grating on silicon waveguide; BS: beam splitter; TPS: thermal phase shifter; W: long silicon waveguide; 2-D WG: two-dimensional grating on silicon waveguide. **(c)** and **(d)** The photographs of the circuit sample and the 2-D WG, respectively.

is used, and the signal and idler photons have different frequencies. Since the quantum interference process in BSM based on linear optics requires that the two input photons should be indistinguishable except the freedom of polarization, such frequency non-degenerate states could not be used in information encoding and decoding.

In this work, we proposed and demonstrated a silicon quantum photonic circuit to realize frequency degenerate polarization entangled Bell state generation at telecom band. It was based on SFWM in the fundamental quasi-TE modes of four silicon waveguides. To generate frequency degenerate biphoton states, a non-degenerate pumping scheme was applied as shown in Fig. 1(a). Stimulated by two pump lights with different frequencies, two pump photons with different frequencies (denoted by ω_{p1} and ω_{p2}) were annihilated, while two photons with the same frequency (denoted by $\omega_{s,i}$) were generated simultaneously through this SFWM process. The energy conservation was satisfied in SFWM, leading to the relation of $\omega_{p1}+\omega_{p2}=2\omega_{s,i}$. The biphoton states generated in the four silicon waveguides were transformed to polarization entangled Bell states by on-chip quantum interference and quantum superposition, and then coupled to optical fibers. By adjusting the phases of the quantum interference and quantum superposition via electrical signals, the output state could be dynamically switched between two polarization entangled Bell states. The performance of the dynamic manipulation was measured, showing its potential on applications requiring dynamic Bell state control and information encoding.

THE SILICON QUANTUM PHOTONIC CIRCUIT

The silicon quantum photonic circuit was fabricated on a SOI substrate with a silicon layer of 220 nm in thickness. Its sketch is shown in Fig. 1(b). It has six input/output ports, denoted by Port 1∼6, respectively. Two pump lights with different frequencies are injected into the photonic circuit through Port 1 and 2, respectively. Both of them are coupled to the fundamental quasi-TE mode of the silicon waveguides by the gratings on silicon waveguides (denoted by WG). Then they are split to four long silicon waveguides (denoted by W1∼4) through three 50:50 beam splitters (denoted by BS 1∼3). All the 50:50 beam splitters on the photonic circuit are realized by 2 × 2 multi-mode interference (MMI) devices. The four long silicon waveguides are used as the nonlinear media of SFWM with the same length of 1 cm. When pump lights propagate along these waveguides, biphoton states are generated by SFWM. The biphoton states generated in W1 and W2 interfere at the fourth 50:50 beam splitter (BS4). The phase of this interference can be adjusted by a thermal phase shifter (TPS2) on W1. The output state of this quantum interference is a superposition of two biphoton states denoted as $|\Psi_{bunch}\rangle$ and $|\Psi_{split}\rangle$[31]. For the photon pairs of $|\Psi_{bunch}\rangle$, the two photons always output from the same port, but which port they select is random. On the contrary, for the photon pairs of $|\Psi_{split}\rangle$, the two photons always output from two different ports, respectively. To realize the polarization entangled Bell state generation, the output state should be adjusted to $|\Psi_{split}\rangle$ by controlling the interference phase through TPS2. This state can be expressed as $|\varphi\rangle_{BS4} = |c, d\rangle_{BS4}$, where "c" and "d" denote the two output ports of BS4, respectively. Similarly, the biphoton states generated in W3 and W4 interfere at the fifth beam splitter (BS5), with proper interference phase control by another thermal phase shifter (TPS3) on W3. The output state of BS5 also can be adjusted to $|\Psi_{split}\rangle$, which can be expressed as $|\varphi\rangle_{BS5} = |c', d'\rangle_{BS5}$, where "c′" and "d′" denote the two output ports of BS5, respectively.

Each output ports of BS4 and BS5 is connected to a two two-dimensional grating on silicon waveguide (2-D WG) as shown in Fig. 1(b). Recently, 2-D WG has become an important component of silicon quantum photonic circuits to realize the conversion between path encoding states and polarization encoding states with high fidelity[29,32-34]. In this circuit, the two 2-D WGs are two output ports of the photonic circuit (Port 5 and 6), by which the generated photon pairs are coupled to two optical fibers. The photons in the two input waveguides of the 2-D WGs would be coupled into two orthogonal polarization modes of the output fiber[35,36], which are denoted by "H" and "V", respectively. By this way, the freedom of paths on the photonic circuit is transformed into the freedom of polarization directions in the two output fibers. The relation between them is defined as Table 1.

Table 1 | The relation between the output ports of BS 4/5 and the polarization directions in output fibers.

Output ports of beam splitters	Output ports of the photonic circuit	Polarization directions in fibers
"c" of BS4	Port 5	H
"d" of BS4	Port 6	V
"c′" of BS5	Port 5	V
"d′" of BS5	Port 6	H

According to this relation, the output biphoton state in the two optical fibers is

$$|\Psi\rangle = \frac{1}{\sqrt{2}}\left(|H,V\rangle + e^{i\alpha}|V,H\rangle\right) \quad (1)$$

It is a maximum polarization entangled state. α is the phase of the quantum superposition, which can be adjusted by the thermal phase shifter (TPS1) between BS 1 and BS 3. Particularly, if α is adjusted to 0 or π, two polarization entangled Bell states can be generated as follows,

$$|\Psi^{\pm}\rangle = \frac{1}{\sqrt{2}}(|H,V\rangle \pm |V,H\rangle) \quad (2)$$

These two biphoton states can be discriminated by BSM based on linear optics.

The circuit was fabricated on a SOI substrate by standard CMOS process. The photographs of the circuit sample and detail of the 2-D WG are shown in Fig. 1(c) and (d), respectively. It is worth noting that Port 3 and 4 are auxiliary input ports connected to BS 2 and BS 3, respectively. They are used to calibrate the thermal phase shifters on the photonic circuit and the experimental setup for the measurement of the output biphoton states. In the measurement, the frequency-degenerate photon pairs would be selected by optical filters before the single photon detectors.

THE EXPERIMENT RESULTS

The indistinguishability of the two photons in photon pairs. In the experiment, the wavelengths of the two pump lights were 1555.7 nm and 1549.3 nm. Firstly, they were combined and injected into Port 3, stimulating SFWM in waveguides W1 and W2. The generated biphoton states interfered at the 50:50 beam splitter BS4. The phase of this interference was controlled by the thermal phase shifter TPS2. The output photons from Port 5 and 6 were coupled to two optical fibers. The generated frequency-degenerate photon pairs were selected by optical filters and detected by two single photon detectors. The central wavelength and full width at half maximum (FWHM) of the optical filters were 1552.5 nm and ∼60 GHz, respectively. Their sideband suppression ratios were both over 100 dB to eliminate the impact of pump lights. The single photon detectors were based on near infrared avalanche photo diodes with efficiencies of ∼20% and dark count rates of ∼100 Hz Fig. 2.(a) shows the coincidence counts of the two single photon detectors under different voltages on TPS2 (It is indicated by the square of the voltage due to Ohm's law). It can be seen that the coincidence counts vary sinusoidally with the square of the voltage, showing the fringe of the quantum interference. It agrees with the theoretical analysis that the output state after BS4 is a superposition of $|\Psi_{\text{bunch}}\rangle$ and $|\Psi_{\text{split}}\rangle$, and the phase of the superposition could be controlled by TPS2. Especially, indicated by the red arrow in Fig. 2(a), the coincidence counts reached its maximum when the voltage was 7.47 V. It corresponds to the situation where the output state only includes $|\Psi_{\text{split}}\rangle$, and the two photons in a pair were separated to Port 5 and 6 respectively.

Under this condition, we took the experiment of Hong-Ou-Mandel (HOM) interference to test the indistinguishability between the photons in generated photon pairs. A 50:50 fiber coupler was connected to the two output fibers. The coincidence counts of the output photons from the fiber coupler were detected by single photon detectors after passing through the optical filters. At one input port of the fiber coupler, a fiber polarization controller was placed to maximize the quantum interference by making the input photons indistinguishable in polarization. At the other input port of the fiber coupler, a variable delay line was placed to adjust the time delay between the two photons in a pair Fig. 2(b) shows the coincidence counts under different time delays. It can be seen that the fringe shows a clear dip when the time delay is close to zero, which is the feature of HOM interference. The red line in the figure is the fitting curve of the HOM dip, under the assumption that the optical filters for the frequency-degenerate photon pairs have rectangular transmission spectra. The raw visibility of the HOM dip is 91.0%. Similarly, we also measured the HOM interference of the photons generated in waveguide W3 and W4 by injecting the pump lights into Port 4. The results are shown in Fig. 2(c). The fringe also shows the clear feature of HOM interference with a raw visibility of 93.9%. The factors impacting the visibilities include counts of noise photons, dark counts and loss difference of the two photons in a pair. These results show that the photons of the generated photon pairs have good indistinguishability, especially in their spectral properties.

The polarization entanglement of the generated photon pairs. The property of polarization entanglement was demonstrated by the experiment of two-photon interference under two non-orthogonal polarization bases. In this experiment, the two pump lights were injected into the photonic circuit from Port 1 and Port 2, respectively. The biphoton states after BS 4 and BS 5 were adjusted to $|\Psi_{\text{split}}\rangle$ by controlling the voltages on TPS2 and TPS3. Under this condition, the frequency-degenerate polarization entangled biphoton state as Eq. (1) would be generated and coupled to two optical fibers from Port 5 and Port 6. The experiment setup is shown in Fig. 3(a). The output photons in the two optical fibers passed through the polarization analyzer and then were detected by the single photon detectors after passing through the optical filters. The polarization analyzer included fiber polarization controllers (FPC1 and FPC2), rotated half-wave plates (HWP1 and HWP2) and fixed polarizers (P1 and P2). The rotated half-wave plates and the fixed polarizers were mounted on benches with fiber collimators. It was collimated by a probe light at 1552.5 nm before the experiment. We measured the single side counts and coincidence counts of the two single photon detectors with varying direction of HWP2 when the direction of HWP1 was set at 0° and 22.5°. The results of single side counts are shown in Fig. 3(b). It can be seen that the single side counts have small fluctuations with varying direction of HWP2. One possible reason for the fluctuation is the unbalanced pump distribution due to the non-ideal splitting ratio of the beam splitters (especially BS1). On the other hand, the polarization-dependent loss (PDL) in the 2-D WGs also may lead to the fluctuations, which could be removed by more complicated 2-D WG designs developed recently[36]. It is worth noting that these non-idealities on the circuit would also impact the results of coincidence counts, which are shown in Fig. 3(c). The raw visibilities of the two sinusoidal fringes are 89.5% and 77.7%, respectively, higher than the criterion

DOI: 10.1016/j.chip.2021.100001

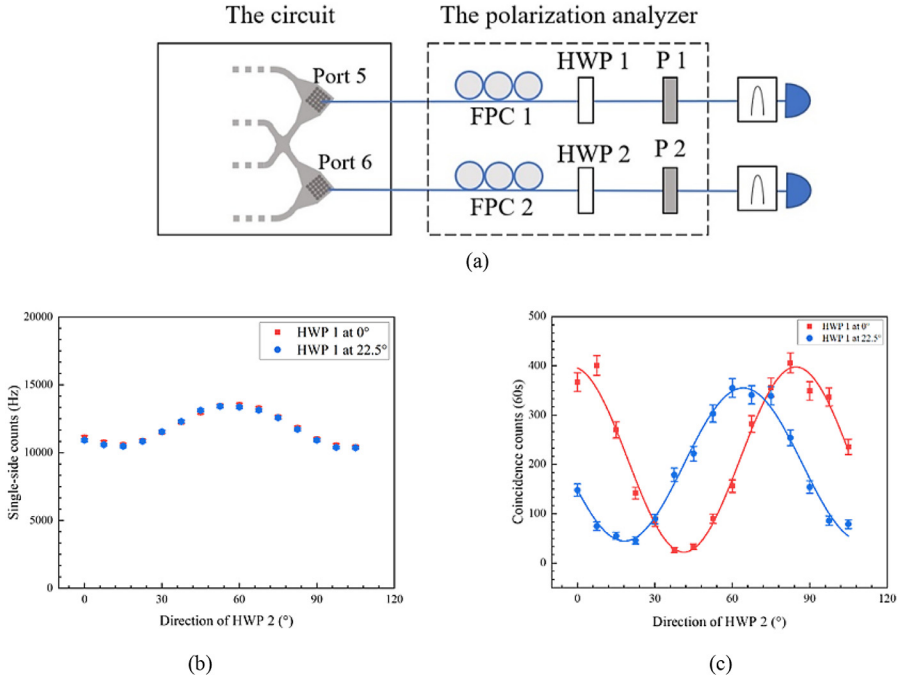

Fig. 2 | The experiment to show the indistinguishability of the two photons in photon pairs (a) Results of quantum interference between the biphoton states generated in W1 and W2 at BS4. **(b)** Results of HOM interference between photons in frequency-degenerate photon pairs generated in W1and W2. **(c)** Results of HOM interference between photons in frequency-degenerate photon pairs generated in W3 and W4. Error bars come from the Poisson statistics of photon counts.

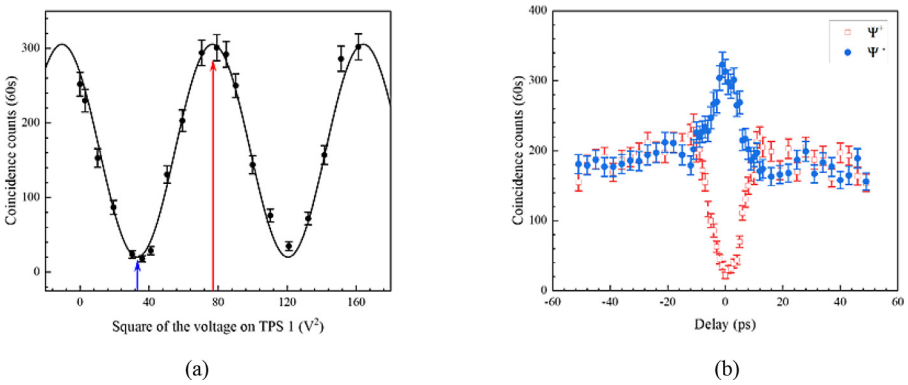

Fig. 3 | Experiment results of two-photon interference under two non-orthogonal polarization bases. (a) Experiment setup. The output photons were collected by two optical fibers and sent to the polarization analyzer. **(b)** Single side counts and **(c)** coincidence counts with varying direction of HWP 2 when the direction of HWP 1 was set at 0° (red squares) and 22.5° (blue circles). Error bars come from the Poisson distribution of photons.

of violation of Bell inequality[23]. Hence, the photons in generated photon pairs are entangled in polarization.

Two polarization Bell states generated by the photonic circuit. The experiment results in Fig. 3 show that the photonic circuit generates telecom-band polarization entangled biphoton state as Eq. (1). In the state, the phase α could be controlled by the thermal phase shifter TPS 1. Hence, two polarization entangled Bell states could be generated under $\alpha=0$ and $\alpha=\pi$, which are shown in Eq. (2). They could be discriminated by a simplified BSM based on a 50:50 fiber coupler. For the photon pairs of $|\Psi^-\rangle$, the two photons in a pair would output from two different ports of the 50:50 fiber coupler respectively, leading to one coincidence count. For the photon pairs of $|\Psi^+\rangle$, the two photons in a pair would output from the same port. Hence, no coincidence count would be recorded. In the experiment, the two output fibers of the photonic circuit connected to the fiber coupler through a variable delay line and a fiber polarization controller, respectively. The output photons from the fiber coupler were detected by the two single photon detectors with the optical filters. Firstly, we optimized the voltage on TPS1, the settings of the variable delay line and the fiber polarization controller to achieve the minimum coincidence counts, which corresponds to $|\Psi^+\rangle$. Then, we measured the coincidence counts under varying voltage on TPS1. The result is shown in Fig. 4(a). It is a sinusoidal curve varying with the square of the voltage on TPS1. The blue arrow and the red arrow indicate the voltage for the minimum and maximum coincidence counts on the fringe, which are the conditions to generate $|\Psi^+\rangle$ and $|\Psi^-\rangle$, respectively. We set the voltage on TPS 1 at these conditions and measure the coincidence counts under different time delays between the two photons in a pair by tuning the variable delay line in both cases. The results are shown in Fig. 4(b). The red hollow squares and blue solid circles in the figure are the results of $|\Psi^+\rangle$ and $|\Psi^-\rangle$, respectively.

DOI: 10.1016/j.chip.2021.100001

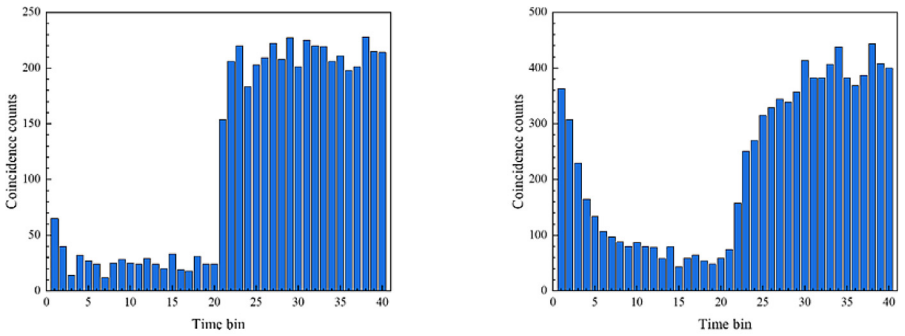

(a) (b)

Fig. 4 | The experimental demonstration of the polarization entangled Bell state generation. (a) The coincidence counts under different voltages on TPS1. The blue and red arrows indicate the voltages for $|\Psi^+\rangle$ and $|\Psi^-\rangle$, respectively. **(b)**The coincidence counts under different time delays of the two photons in a pair at the 50:50 fiber coupler. The results of $|\Psi^+\rangle$ and $|\Psi^-\rangle$ are shown by the red hollow squares and the blue solid circles, respectively.

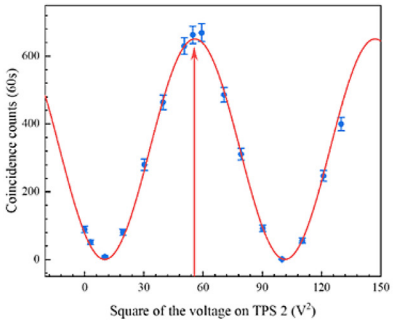

(a)

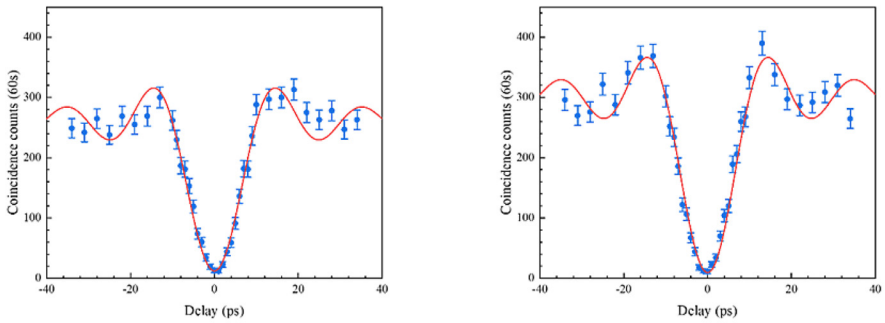

(b) (c)

Fig. 5 | The dynamic manipulation of the two polarization entangled Bell states. (a) the results under a square wave repetition rate of 1 kHz and a counting time of 600 s. **(b)** the results under a square wave repetition rate of 20 kHz and a counting time of 1200s.

It can be seen that they are almost the same when the time delay is large, since no quantum interference took place in this condition. On the other hand, a significant difference between them appears when the time delay is close to zero, showing that the two biphoton states can be discriminated by the simplified BSM. The raw visibility of the two fringes is 87.2%, which is calculated by

$$F = \frac{C_{\max} - C_{\min}}{C_{\max} + C_{\min}} \tag{3}$$

Where C_{max} and C_{min} denote the maximum coincidence count for $|\Psi^-\rangle$ and minimum coincidence count for $|\Psi^+\rangle$, respectively. Since generation and measurement of these polarization entangled Bell states need more complicated processes of on-chip thermal phase shifter adjustment and polarization collimation in the measurement system, the measurement is more sensitive to the environment variation than that of HOM interference. It can be seen that the measured F is a little lower than the raw visibilities of HOM interference shown in Fig. 2. However, these results clearly show that two polarization entangled Bell states, $|\Psi^+\rangle$ and $|\Psi^-\rangle$, were generated successfully by the electrical control on the photonic circuit. They can be discriminated by BSM based on linear optics with good fidelity.

Dynamic manipulation of the two polarization entangled Bell states. Dynamic manipulation of polarization entangled Bell states has important applications on quantum communication and quantum information processing requiring quantum encoding, such as quantum dense coding and quantum secure direct communication, etc. The output biphoton state of the silicon quantum photonic circuit in this work can be switched dynamically between $|\Psi^+\rangle$ and $|\Psi^-\rangle$. We demonstrated this function by the sim-

plified BSM. A square wave signal is applied on TPS1, the voltages in the first and second halves of a period were set at the voltage for $|\Psi^+\rangle$ and $|\Psi^-\rangle$, respectively. The coincidence counts of the output photons from the fiber coupler were measured under the optimized condition by controlling the variable delay line and the fiber polarization controller. A period of the square wave was split into 40 time bins, and coincidence events in different periods were counted in these time bins. The histograms shown in Fig. 5(a) and (b) are the experimental results when the repetition rates of the square wave signal were 1 kHz and 20 kHz. In these figures, each bar indicates the coincidence counts in a specific bin. It can be seen that the coincidence counts in the first and second halves of a period have significant difference under a repetition rate of 1 kHz, indicating that the output biphoton state was switched between $|\Psi^+\rangle$ and $|\Psi^-\rangle$ by the square wave signal successfully. When the repetition rate increases to 20 kHz, the transient process of the biphoton state manipulation can be observed. It shows that the photonic circuit supports a dynamic biphoton state modulation of several tens of kHz. The manipulation speed is typical for the silicon photonic circuits with thermal phase shifters [37,38]. To our knowledge, it is the first demonstration of the on-chip dynamic manipulation of entangled biphoton states. It is worth noting that higher modulation speed could be expected if phase shifters based on electro-optic effect are used in this photonic circuit design. Recent developments of hybrid silicon and lithium niobate devices show great potential on this application [39].

CONCLUSIONS

In this work, generation and dynamic manipulation of polarization entangled Bell states were realized by a silicon quantum photonic circuit. In the photonic circuit, biphoton states were generated in four long silicon waveguides by SFWM. They were transformed to polarization entangled Bell states by quantum interference and quantum superposition, and then outputted through optical fibers. The property of polarization entanglement in the output states was demonstrated by two-photon interference under two non-orthogonal polarization bases, with raw fringe visibilities of 89.5% and 77.7%, respectively. The output state can be switched between two polarization entangled Bell states, $|\Psi^+\rangle$ and $|\Psi^-\rangle$, through the electrical signal applied on thermal phase shifters. It was demonstrated by a simplified BSM experiment, showing a visibility of 87.2% in the coincidence measurements of $|\Psi^+\rangle$ and $|\Psi^-\rangle$. By applying square wave signal on the thermal phase shifter, the dynamic process of the Bell state modulation was observed. Experiment results showed that the silicon quantum photonic circuit supports a modulation rate of several tens kHz, showing its potential on applications of quantum communication and quantum information processing requiring Bell state encoding and dynamic control.

METHODS

Experimental setup. In the experiment, the wavelengths of the two pump lights were 1555.7 nm and 1549.3 nm, respectively. Firstly, they were combined and injected into Port 3, stimulating SFWM in waveguides W1 and W2. The generated biphoton states interfered at the 50:50 beam splitter BS4. The phase of this interference was controlled by the thermal phase shifter TPS2. The output photons from Ports 5 and 6 were coupled to two optical fibers. The generated frequency-degenerate photon pairs were selected by optical filters and detected by two single photon detectors. The central wavelength and full width at half maximum (FWHM) of the optical filters were 1552.5 nm and ~60 GHz, respectively. Their sideband suppression ratios were both over 100 dB to eliminate the impact of pump lights. The single photon detectors were based on near-infrared avalanche photo diodes with efficiencies of ~20% and dark count rates of ~100 Hz.

On-chip generation of $|\Psi_{\text{split}}\rangle$. Figure 5(a) shows the coincidence counts of the two single photon detectors under different voltages on TPS2 (indicated by the square of the voltage due to Ohm's law). It can be seen that the coincidence counts vary sinusoidally with the square of the voltage, showing the fringe of the quantum interference. It agrees with the theoretical analysis that the output state after BS4 is a superposition of $|\Psi_{\text{bunch}}\rangle$ and $|\Psi_{\text{split}}\rangle$, and the phase of the superposition could be controlled by TPS2. In particular, as indicated by the red arrow in Fig. 5(a), the coincidence counts reached its maximum when the voltage was 7.47V. It corresponds to the situation where the output state only included $|\Psi_{\text{split}}\rangle$, and the two photons in a pair were separated to Ports 5 and 6 respectively.

The indistinguishability of the two photons in photon pairs. Under the condition of on-chip generation of $|\Psi_{\text{split}}\rangle$, we performed the experiment of Hong-Ou-Mandel (HOM) interference to test the indistinguishability between the photons in generated photon pairs. A 50:50 fiber coupler was connected to the two output fibers. The coincidence counts of the output photons from the fiber coupler were detected by single photon detectors after passing through the optical filters. At one input port of the fiber coupler, a fiber polarization controller was placed to maximize the quantum interference by making the input photons indistinguishable in polarization. At the other input port of the fiber coupler, a variable delay line was placed to adjust the time delay between the two photons in a pair. Figure 5(b) shows the coincidence counts under different time delays. It can be seen that the fringe shows a clear dip when the time delay is close to zero, which is the feature of HOM interference. The red line in the figure is the fitting curve of the HOM dip, under the assumption that the optical filters for the frequency-degenerate photon pairs have rectangular transmission spectra. The raw visibility of the HOM dip is 91.0%. Similarly, we also measured the HOM interference of the photons generated in waveguide W3 and W4 by injecting the pump lights into Port 4. The results are shown in Fig. 5(c). The fringe also shows clear feature of HOM interference with a raw visibility of 93.9%. The factors impacting the visibilities include counts of noise photons, dark counts and loss difference of the two photons in a pair. These results show that the photons of the generated photon pairs have good indistinguishability, especially in their spectral properties.

REFERENCES

1. Bogdanov, S., Shalaginov, M. Y., Boltasseva, A. & Shalaev, V. M. Material platforms for integrated quantum photonics. *Opt. Mater. Express* **7**, 111–132 (2017). https://doi.org/10.1364/ome.7.000111.
2. Orieux, A. & Diamanti, E. Recent advances on integrated quantum communications. *J. Opt.* **18**, 8 (2016). https://doi.org/10.1088/2040-8978/18/8/083002.
3. Silverstone, J. W., Bonneau, D., O'Brien, J. L. & Thompson, M. G. Silicon quantum photonics. *IEEE J. Sel. Top. Quantum Electron.* **22**, 390–402 (2016). https://doi.org/10.1109/jstqe.2016.2573218.
4. Wang, J., Paesani, S., Ding, Y., Santagati, R., Skrzypczyk, P., Salavrakos, A., Tura, J., Augusiak, R., Mancinska, L., Bacco, D., Bonneau, D., Silverstone, J. W., Gong, Q., Acin, A., Rottwitt, K., Oxenlowe, L. K., O'Brien, J. L., Laing, A. & Thompson, M. G. Multidimensional quantum entanglement with large-scale integrated optics. *Science* **360**, 285–291 (2018). https://doi.org/10.1126/science.aar7053.
5. Wang, J., Sciarrino, F., Laing, A. & Thompson, M. G. Integrated photonic quantum technologies. *Nat. Photonics* **14**, 273–284 (2020). https://doi.org/10.1038/s41566-019-0532-1.
6. Sharping, J. E., Lee, K. F., Foster, M. A., Turner, A. C., Schmidt, B. S., Lipson, M., Gaeta, A. L. & Kumar, P. Generation of correlated photons in nanoscale silicon waveguides. *Opt. Express* **14**, 12388–12393 (2006). https://doi.org/10.1364/oe.14.012388.
7. Takesue, H., Fukuda, H., Tsuchizawa, T., Watanabe, T., Yamada, K., Tokura, Y. & Itabashi, S.-I. Generation of polarization entangled photon pairs using silicon wire waveguide. *Opt. Express* **16**, 5721–5727 (2008). https://doi.org/10.1364/oe.16.005721.
8. Li, Y.-H., Zhou, Z.-Y., Feng, L.-T., Fang, W.-T., Liu, S.-L., Liu, S.-K., Wang, K., Ren, X.-F., Ding, D.-S., Xu, L.-X. & Shi, B.-S. On-chip multiplexed multiple entan-

glement sources in a single silicon nanowire. *Phys. Rev. Appl.* **7**, 064005 (2017). https://doi.org/10.1103/PhysRevApplied.7.064005.
9. Azzini, S., Grassani, D., Strain, M. J., Sorel, M., Helt, L. G., Sipe, J. E., Liscidini, M., Galli, M. & Bajoni, D. Ultra-low power generation of twin photons in a compact silicon ring resonator. *Opt. Express* **20**, 23100–23107 (2012). https://doi.org/10.1364/oe.20.023100.
10. Guo, Y., Zhang, W., Dong, S., Huang, Y. & Peng, J. Telecom-band degenerate-frequency photon pair generation in silicon microring cavities. *Opt. Lett.* **39**, 2526–2529 (2014). https://doi.org/10.1364/ol.39.002526.
11. Jiang, W. C., Lu, X., Zhang, J., Painter, O. & Lin, Q. Silicon-chip source of bright photon pairs. *Opt. Express* **23**, 20884–20904 (2015). https://doi.org/10.1364/oe.23.020884.
12. Feng, L.-T., Guo, G.-C. & Ren, X.-F. Progress on integrated quantum photonic sources with silicon. *Adv. Quantum Technol.* **3**, 190058 (2020). https://doi.org/10.1002/qute.201900058.
13. Gentry, C. M., Shainline, J. M., Wade, M. T., Stevens, M. J., Dyer, S. D., Zeng, X., Pavanello, F., Gerrits, T., Nam, S. W., Mirin, R. P. & Popovic, M. A. Quantum-correlated photon pairs generated in a commercial 45 nm complementary metal-oxide semiconductor microelectronic chip. *Optica* **2**, 1065–1071 (2015). https://doi.org/10.1364/optica.2.001065.
14. Bunandar, D., Lentine, A., Lee, C., Cai, H., Long, C. M., Boynton, N., Martinez, N., DeRose, C., Chen, C., Grein, M., Trotter, D., Starbuck, A., Pomerene, A., Hamilton, S., Wong, F. N. C., Camacho, R., Davids, P., Urayama, J. & Englund, D. Metropolitan quantum key distribution with silicon photonics. *Phys. Rev. X* **8**, 021009 (2018). https://doi.org/10.1103/PhysRevX.8.021009.
15. Harris, N. C., Bunandar, D., Pant, M., Steinbrecher, G. R., Mower, J., Prabhu, M., Baehr-Jones, T., Hochberg, M. & Englund, D. Large-scale quantum photonic circuits in silicon. *Nanophotonics* **5**, 456–468 (2016). https://doi.org/10.1515/nanoph-2015-0146.
16. Harris, N. C., Steinbrecher, G. R., Prabhu, M., Lahini, Y., Mower, J., Bunandar, D., Chen, C., Wong, F. N. C., Baehr-Jones, T., Hochberg, M., Lloyd, S. & Englund, D. Quantum transport simulations in a programmable nanophotonic processor. *Nat. Photonics* **11**, 447–452 (2017). https://doi.org/10.1038/nphoton.2017.95.
17. Qiang, X., Zhou, X., Wang, J., Wilkes, C. M., Loke, T., O'Gara, S., Kling, L., Marshall, G. D., Santagati, R., Ralph, T. C., Wang, J. B., O'Brien, J. L., Thompson, M. G. & Matthews, J. C. F. Large-scale silicon quantum photonics implementing arbitrary two-qubit processing. *Nat. Photonics* **12**, 534–539 (2018). https://doi.org/10.1038/s41566-018-0236-y.
18. ResearchMatsuda, N. Photonics & Takesue, H. Generation and manipulation of entangled photons on silicon chips. *Nanophotonics* **5**, 440–455 (2016). https://doi.org/10.1515/nanoph-2015-0148.
19. Wakabayashi, R., Fujiwara, M., Yoshino, K.-I., Nambu, Y., Sasaki, M. & Aoki, T. Time-bin entangled photon pair generation from Si micro-ring resonator. *Opt. Express* **23**, 1103–1113 (2015). https://doi.org/10.1364/oe.23.001103.
20. Grice, W. P. Arbitrarily complete Bell-state measurement using only linear optical elements. *Phys. Rev. A* **84**, 042331 (2011). https://doi.org/10.1103/PhysRevA.84.042331.
21. Mattle, K., Weinfurter, H., Kwiat, P. G. & Zeilinger, A. Dense coding in experimental quantum communication. *Phys. Rev. Lett.* **76**, 4656–4659 (1996). https://doi.org/10.1103/PhysRevLett.76.4656.
22. Bostrom, K. & Felbinger, T. Deterministic secure direct communication using entanglement. *Phys. Rev. Lett.* **89**, 4 (2002). https://doi.org/10.1103/PhysRevLett.89.187902.
23. Kwiat, P. G., Mattle, K., Weinfurter, H., Zeilinger, A., Sergienko, A. V. & Shih, Y. H. New high-intensity source of polarization-entangled photon pairs. *Phys. Rev. Lett.* **75**, 4337–4341 (1995). https://doi.org/10.1103/PhysRevLett.75.4337.
24. Kim, Y. H., Kulik, S. P. & Shih, Y. H. Bell-state preparation using pulsed nondegenerate two-photon entanglement. *Phys. Rev. A* **63**, 060301 (2001). https://doi.org/10.1103/PhysRevA.63.060301.
25. Jin, H., Liu, F. M., Xu, P., Xia, J. L., Zhong, M. L., Yuan, Y., Zhou, J. W., Gong, Y. X., Wang, W. & Zhu, S. N. On-chip generation and manipulation of entangled photons based on reconfigurable lithium-niobate waveguide circuits. *Phys. Rev. Lett.* **113**, 103601 (2014). https://doi.org/10.1103/PhysRevLett.113.103601.
26. Horn, R. T., Kolenderski, P., Kang, D., Abolghasem, P., Scarcella, C., Della Frera, A., Tosi, A., Helt, L. G., Zhukovsky, S. V., Sipe, J. E., Weihs, G., Helmy, A. S. & Jennewein, T. Inherent polarization entanglement generated from a monolithic semiconductor chip. *Sci. Rep.* **3**, 2314 (2013). https://doi.org/10.1038/srep02314.
27. Zhang, X., Bell, B. A., Mahendra, A., Xiong, C., Leong, P. H. W. & Eggleton, B. J. Integrated silicon nitride time-bin entanglement circuits. *Opt. Lett.* **43**, 3469–3472 (2018). https://doi.org/10.1364/ol.43.003469.
28. Matsuda, N., Jeannic, H. Le, Fukuda, H., Tsuchizawa, T., Munro, W. J., Shimizu, K., Yamada, K., Tokura, Y. & Takesue, H. A monolithically integrated polarization entangled photon pair source on a silicon chip. *Sci. Rep.* **2**, 817 (2012). https://doi.org/10.1038/srep00817.
29. Olislager, L., Safioui, J., Clemmen, S., Huy, K. P., Bogaerts, W., Baets, R., Emplit, P. & Massar, S. Silicon-on-insulator integrated source of polarization-entangled photons. *Opt. Lett.* **38**, 1960–1962 (2013). https://doi.org/10.1364/ol.38.001960.
30. Harada, K.-i., Takesue, H., Fukuda, H., Tsuchizawa, T., Watanabe, T., Yamada, K., Tokura, Y. & Itabashi, S.-i. Frequency and polarization characteristics of correlated photon-pair generation using a silicon wire waveguide. *IEEE J. Sel. Top. Quantum Electron.* **16**, 325–331 (2010). https://doi.org/10.1109/jstqe.2009.2023338.
31. Silverstone, J. W., Bonneau, D., Ohira, K., Suzuki, N., Yoshida, H., Iizuka, N., Ezaki, M., Natarajan, C. M., Tanner, M. G., Hadfield, R. H., Zwiller, V., Marshall, G. D., Rarity, J. G., O'Brien, J. L. & Thompson, M. G. On-chip quantum interference between silicon photon-pair sources. *Nat. Photonics* **8**, 104–108 (2014). https://doi.org/10.1038/nphoton.2013.339.
32. Wang, J., Bonneau, D., Villa, M., Silverstone, J. W., Santagati, R., Miki, S., Yamashita, T., Fujiwara, M., Sasaki, M., Terai, H., Tanner, M. G., Natarajan, C. M., Hadfield, R. H., O'Brien, J. L. & Thompson, M. G. Chip-to-chip quantum photonic interconnect by path-polarization interconversion. *Optica* **3**, 407–413 (2016). https://doi.org/10.1364/optica.3.000407.
33. Sibson, P., Kennard, J. E., Stanisic, S., Erven, C., O'Brien, J. L. & Thompson, M. G. Integrated silicon photonics for high-speed quantum key distribution. *Optica* **4**, 172–177 (2017). https://doi.org/10.1364/optica.4.000172.
34. Llewellyn, D., Ding, Y., Faruque, I. I., Paesani, S., Bacco, D., Santagati, R., Qian, Y.-J., Li, Y., Xiao, Y.-F., Huber, M., Malik, M., Sinclair, G. F., Zhou, X., Rottwitt, K., O'Brien, J. L., Rarity, J. G., Gong, Q., Oxenlowe, L. K., Wang, J. & Thompson, M. G. Chip-to-chip quantum teleportation and multi-photon entanglement in silicon. *Nat. Phys.* **16**, 148–153 (2020). https://doi.org/10.1038/s41567-019-0727-x.
35. Taillaert, D., Chong, H., Borel, P. I., Frandsen, L. H., De La Rue, R. M. & Baets, R. A compact two-dimensional grating coupler used as a polarization splitter. *IEEE Photon. Technol. Lett.* **15**, 1249–1251 (2003). https://doi.org/10.1109/lpt.2003.816671.
36. Marchetti, R., Lacava, C., Carroll, L., Gradkowski, K. & Minzioni, P. Coupling strategies for silicon photonics integrated chips Invited. *Photon. Res* **7**, 201–239 (2019). https://doi.org/10.1364/prj.7.000201.
37. Song, J., Fang, Q., Tao, S. H., Liow, T. Y., Yu, M. B., Lo, G. Q. & Kwong, D. L. Fast and low power Michelson interferometer thermo-optical switch on SOI. *Opt. Express* **16**, 15304–15311 (2008). https://doi.org/10.1364/oe.16.015304.
38. Densmore, A., Janz, S., Ma, R., Schmid, J. H., Xu, D.-X., Delage, A., Lapointe, J., Vachon, M. & Cheben, P. Compact and low power thermo-optic switch using folded silicon waveguides. *Opt. Express* **17**, 10457–10465 (2009). https://doi.org/10.1364/oe.17.010457.
39. He, M., Xu, M., Ren, Y., Jian, J., Ruan, Z., Xu, Y., Gao, S., Sun, S., Wen, X., Zhou, L., Liu, L., Guo, C., Chen, H., Yu, S., Liu, L. & Cai, X. High-performance hybrid silicon and lithium niobate Mach-Zehnder modulators for 100 Gbit s(-1) and beyond. *Nat. Photonics* **13**, 359–364 (2019). https://doi.org/10.1038/s41566-019-0378-6.

MISCELLANEA

Funding National Key R&D Program of China (2017YFA0303704,), Natural Science Foundation of Beijing (Z180012), National Natural Science Foundation of China (61875101, 91750206), Beijing Academy of Quantum Information Science (Y18G26), Tsinghua Initiative Scientific Research Program.

Data availability Data underlying the results presented in this paper are not publicly available at this time but may be obtained from the authors upon reasonable request.

Author contributions Wei Zhang and Lingjie Yu proposed the silicon quantum photonic circuit design and were responsible for the chip fabrication. Dongning Liu, Jingyuan Zheng and Lingjie Yu performed experiments and analyzed data. Wei Zhang, Dongning Liu and Lingjie Yu wrote the manuscript. Yidong Huang revised the manuscript and supervised the project. Xue Feng, Fang Liu, Kaiyu Cui contributed to experiment design and the revision of the manuscript.

Declaration of Competing Interest The authors declare no competing interests.